
Learning Interface Conditions in Domain Decomposition Solvers

Ali Taghibakhshi

Mechanical Science and Engineering
University of Illinois Urbana-Champaign
Urbana, IL 61801, USA
alit2@illinois.edu

Nicolas Nytko

Computer Science
University of Illinois Urbana-Champaign
Urbana, IL 61801, USA
nnytko2@illinois.edu

Tareq Zaman

Scientific Computing Program
Memorial University of Newfoundland
and Labrador
St. John's, NL, Canada
tzaman@mun.ca

Scott MacLachlan

Mathematics and Statistics
Memorial University of Newfoundland
and Labrador
St. John's, NL, Canada
smacLachlan@mun.ca

Luke Olson

Computer Science
University of Illinois Urbana-Champaign
Urbana, IL 61801, USA
lukeo@illinois.edu

Matthew West

Mechanical Science and Engineering
University of Illinois Urbana-Champaign
Urbana, IL 61801, USA
mwest@illinois.edu

Abstract

Domain decomposition methods are widely used and effective in the approximation of solutions to partial differential equations. Yet the *optimal* construction of these methods requires tedious analysis and is often available only in simplified, structured-grid settings, limiting their use for more complex problems. In this work, we generalize optimized Schwarz domain decomposition methods to unstructured-grid problems, using Graph Convolutional Neural Networks (GCNNs) and unsupervised learning to learn optimal modifications at subdomain interfaces. A key ingredient in our approach is an improved loss function, enabling effective training on relatively small problems, but robust performance on arbitrarily large problems, with computational cost linear in problem size. The performance of the learned linear solvers is compared with both classical and optimized domain decomposition algorithms, for both structured- and unstructured-grid problems.

1 Introduction

Domain decomposition methods (DDMs) Toselli and Widlund [2005], Quarteroni and Valli [1999], Dolean et al. [2015] are highly effective in solving the linear and nonlinear systems of equations that arise from the numerical approximation of solutions to partial differential equations (PDEs). While most effective on elliptic boundary-value problems, DDMs can also be applied to nonlinear problems, either using their nonlinear variants, or successively solving linearizations. Time-dependent problems are normally solved by using a time stepping algorithm in the time domain for implicit methods, which require the solution of a spatial problem for each time step. Of these methods, Schwarz methods are particularly popular given their relative simplicity and ease of parallelization. The common theme is to break the global problem into subproblems, derived either by projection or by

discretizing the same PDE over a physical subdomain, and to use solutions on the subdomains as a preconditioner for the global discretization. Classical Schwarz methods generally make use of Dirichlet or Neumann boundary conditions for these subdomain problems, while Optimized Schwarz Methods (OSMs) aim to improve the convergence of the algorithm by using more general interface conditions Gander et al. [2000]. Notably, Gander and Kwok [2011] demonstrates that optimal, but non-local, interface conditions exist for more general decompositions.

Much of the OSM literature considers only one-level additive Schwarz methods, although multilevel extensions do exist. For one-level methods (i.e., domain decomposition approaches without a “coarse grid”), restricted additive Schwarz (RAS) approaches Cai and Sarkis [1999] are arguably the most common; optimized restricted additive Schwarz (ORAS) methods are considered in St-Cyr et al. [2007]. The OSM idea has also been extended to asynchronous Schwarz methods Magoulès et al. [2017], where the computations on each subdomain are done using the newest information available in a parallel computing environment without synchronizing the solves on each subdomain.

With a recent focus on machine learning (ML) techniques for solving PDE systems Raissi et al. [2019], Li et al. [2020a], there is also effort to apply learning-based methods to improve the performance of iterative solvers for PDEs, including DDM and algebraic multigrid (AMG) methods. Within AMG methods, ML techniques have been applied to learning interpolation operators Greenfeld et al. [2019], Luz et al. [2020] and to coarse-grid selection in reduction-based AMG Taghibakhshi et al. [2021]. Of particular note here is the loss function employed in Greenfeld et al. [2019], Luz et al. [2020], where they use unsupervised learning to train a graph neural network to minimize the Frobenius norm of the error-propagation operator of their iterative method. Within DDM, significant effort has been invested in combining ML techniques with DDM, as in Heinlein et al. [2021], where two main families of approaches are given: 1) using ML within classical DDM methods to improve convergence, and 2) using deep neural networks, such as Physics Informed Neural Networks (PINNs) Raissi et al. [2019], as a discretization module and solver for DDM problems. In Heinlein et al. [2019], a fully connected neural network is used to predict the geometric locations of constraints for coarse space enhancements in an adaptive Finite Element Tearing and Interconnecting-Dual Primal (FETI-DP) method. Using the continuous formulation of DDM, the so-called D3M Li et al. [2019] uses a variational deep learning solver, implementing local neural networks on physical subdomains in a parallel fashion. Likewise, Deep-DDM Li et al. [2020b] utilizes PINNs to discretize and solve DDM problems, with coarse space corrections Mercier et al. [2021] being used to improve scalability.

In this paper, we advance DDM-based solvers by developing a framework for learning optimized Schwarz preconditioners. A key aspect of this is reconsidering the loss function to use a more effective relaxation of the ideal objective function than Frobenius norm minimization Greenfeld et al. [2019], Luz et al. [2020]. Moreover, the approach introduced here offers an opportunity to reconsider existing limitations of optimized Schwarz methods, where optimal parameter choice is based on Fourier analysis and requires a highly regular subdomain structure, such as in the classical cases of square domains split into two equal subdomains or into regular grids of square subdomains. Our framework learns the optimized Schwarz parameters via training on small problem sizes, in a way that generalizes effectively to large problems, and in a way that allows us to consider both irregular domains and unstructured grids, with no extraordinary limitations on subdomain shape. Furthermore, the evaluation time of our algorithm scales linearly with problem size. This allows significant freedom in defining optimized Schwarz methods, in comparison to classical approaches, allowing us to explore the potential benefits of optimized Schwarz over classical (restricted) additive methods on unstructured grids for the first time.

2 Background

Let $\Omega \subset \mathbb{R}^2$ be an open set, and consider the positive-definite Helmholtz problem

$$Lu = (\eta - \Delta)u = f \quad \text{in } \Omega, \quad (1)$$

with inhomogeneous Dirichlet conditions imposed on the boundary $\partial\Omega$. In (1), the parameter $\eta > 0$ represents a *shift* in the Helmholtz problem. In the numerical results below, we consider both finite-difference discretizations of (1) on regular grids, as well as piecewise linear finite-element (FE) discretizations on arbitrary triangulations. In both cases, we denote the set of degrees of freedom as D , and note that these are in a one-to-one correspondence with the nodes of the underlying mesh. Consider a decomposition of D into non-overlapping subdomains $D_i^0, i \in \{1, 2, \dots, S\}$ such that

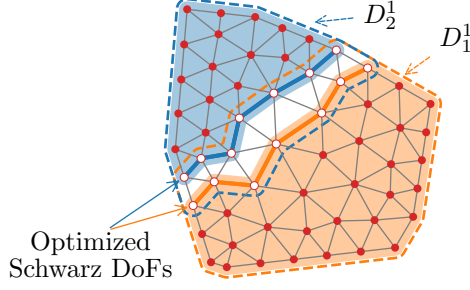


Figure 1: Two subdomains with overlap $\delta = 1$ on a 58-node unstructured grid. The blue and orange shading denotes the original non-overlapping partitions (D_1^0 and D_2^0), while the blue and orange dashed outlines show the overlapping subdomains (D_1^1 and D_2^1). Nodes belonging to only one subdomain are marked with a solid circle, while those in white belong to both subdomains. The connections in the boundary matrices L_1 and L_2 are denoted by the edges shaded in blue (for L_1) and orange (for L_2).

each node is contained within exactly one subdomain D_i^0 , yielding $\cup D_i^0 = D$. In this subdomain notation, the superscript denotes the amount of overlap in the subdomains, which is zero for the non-overlapping subdomains that we first consider. Let R_i^0 be the restriction operator onto the set of degrees of freedom (DoFs) in D_i^0 , and let $(R_i^0)^T$ be the corresponding extension operator from D_i^0 into set D . Then, an FE discretization of the Helmholtz problem leads to a linear system of the form $Ax = b$, where A is the global stiffness matrix and $A_i^0 = R_i^0 A (R_i^0)^T$ is the subdomain stiffness matrix for D_i^0 . We note that alternate definitions to the Galerkin projection for A_i^0 are possible, and are commonly considered in optimized Schwarz settings (as noted below).

In the case of restricted additive Schwarz (RAS) Cai and Sarkis [1999], the subdomains are extended to allow for overlap: nodes near the “boundary” of their subdomain are potentially included in two or more subdomains. We denote the amount of overlap by $\delta \in \mathbb{N}$, defining subdomains D_i^δ recursively, by $D_i^\delta = D_i^{\delta-1} \cup \{j \mid a_{kj} \neq 0 \text{ and } k \in D_i^{\delta-1}\}$ for $\delta > 0$. The conventional RAS preconditioner is defined as

$$M_{\text{RAS}} = \sum_{i=1}^S (\tilde{R}_i^\delta)^T (A_i^\delta)^{-1} R_i^\delta, \quad (2)$$

where R_i^δ is the standard restriction operator to subdomain Ω_i^δ , \tilde{R}_i^δ is a modified restriction operator from D to the DoFs in D_i^δ that takes nonzero values only for DoFs in D_i^0 , and $A_i^\delta = (R_i^\delta)^T A R_i^\delta$. Figure 1 shows an example unstructured grid with two subdomains and overlap $\delta = 1$.

In an optimized Schwarz setting, we modify the subdomain systems, A_i^δ . Rather than using a Galerkin projection onto D_i^δ , we rediscretize (1) over the subdomain of Ω corresponding to these DoFs, imposing a Robin-type boundary condition on the boundary of the subdomain. We define this matrix to be $\tilde{A}_i^\delta = A_i + L_i$, where A_i is the term resulting from discretization of (1) with Neumann boundary conditions, and L_i is additional the term resulting from the Robin-type condition, as in:

$$\text{Dirichlet: } u = g_D(x), \quad \text{Neumann: } \vec{n} \cdot \nabla u = g_N(x), \quad \text{Robin: } \alpha u + \vec{n} \cdot \nabla u = g_R(x), \quad (3)$$

where \vec{n} is the outward normal to the edge on the boundary and g denotes inhomogeneous data.

The matrix L_i has the same dimensions as A_i , so that \tilde{A}_i^δ is well-defined. However, it has a significantly different sparsity pattern, with nonzero entries only in rows/columns corresponding to nodes on the boundary of subdomain D_i^δ . In practice, we identify a cycle or path in the graph corresponding to A_i with the property that every node in the cycle is on the boundary of D_i^δ but not the boundary of D (the discretized domain), and then restrict the nonzeros in L_i to the entries corresponding to the edges in this cycle/path (including self-edges, corresponding to entries on the diagonal of L_i).

Using this notation, the ORAS preconditioner can be written as

$$M_{\text{ORAS}} = \sum_{i=1}^S (\tilde{R}_i^\delta)^T (\tilde{A}_i^\delta)^{-1} R_i^\delta. \quad (4)$$

Our aim is to learn the values in the matrices L_i , aiming to outperform the classical choices of these values predicted by Fourier analysis, in the cases where those values are known, and to learn suitable values for cases, such as finite-element discretizations on unstructured grids, where no known optimized Schwarz parameters exist. We optimize the values for the case of stationary (Richardson) iteration, but evaluate the performance of the resulting methods both as stationary iterations and as preconditioners for FGMRES.

Graph Neural Networks (GNNs): Applying learning techniques to graph structured data necessitates stepping beyond multilayer perceptron (MLP) and conventional convolutional neural networks (CNN) to a type of network that leverages the underlying graph nature of the problem, namely graph convolutional neural networks (GCNNs). GCNNs are typically divided into two categories: spectral and spatial Wu et al. [2020]. Spectral GCNNs, first introduced by Bruna et al. Bruna et al. [2013], consider a graph Laplacian eigenbasis and define convolution as diagonal operators. As such, spectral GCNN methods suffer from time complexity problems due to the necessity for the eigendecomposition of the Laplacian matrix. Nevertheless, in follow-up work Defferrard et al. [2016], Kipf and Welling [2016], remedies have been proposed to mitigate this. Unlike spectral methods, spatial GCNNs consider local propagation of information in graph domains as a convolution graph. One popular framework is the message passing neural network (MPNN) Gilmer et al. [2017], which is based on sharing information among neighbor nodes in each round of a convolution pass. This has been generalized Battaglia et al. [2018] by introducing a configurable graph network block structure consisting of node and edge convolution modules and a global attribute. In an effort to alleviate computational complexity of GCNNs Du et al. [2017], topology adaptive graph convolution networks (TAGCN) can be constructed by defining learnable filters. This is not only computationally simpler, but also allows for adapting to the topology of the graphs when scanning them for convolution.

3 Method

3.1 Optimization problem and the loss function

Throughout this paper, we use $\|\cdot\|$ to denote the ℓ^2 norm of a matrix or vector, $\|A\|_F$ for the Frobenius norm of A , and $\rho(A)$ as the spectral radius of A . The optimization problem that we seek to solve is to find optimal values for the entries in the matrices L_i , constrained by given sparsity patterns, to minimize $\rho(T)$, where $T = I - M_{\text{ORAS}}A$ is the error-propagation operator for the stationary iteration corresponding to M_{ORAS} defined in (4). The spectral radius $\rho(T)$ corresponds to the *asymptotic convergence factor* of the stationary iteration, giving a bound on the asymptotic convergence of the method. Formally defined in terms of the extremal eigenvalue of $T^T T$ (since T is not symmetric), direct minimization of $\rho(T)$ is difficult since backpropagation of an eigendecomposition is numerically unstable Wang et al. [2019]. To overcome this, Luz et al. Luz et al. [2020] propose to relax the minimization of $\rho(T)$ (for a similar AMG preconditioner) to minimizing the Frobenius norm of T , $\|T\|_F$. In our experiments, however, we find that this is insufficient, leading to preconditioners that do not scale. One reason is that while the Frobenius norm is an upper bound on the spectral radius, it does not appear to be a suitably “tight” bound for use in this context (see Section 4.2 and Figure 6). Instead, we use a relaxation inspired by Gelfand’s formula, that $\rho(T) = \lim_{K \rightarrow \infty} \|T^K\|^{\frac{1}{K}}$, and the common bound that

$$\rho(T) \leq \|T^K\|^{\frac{1}{K}} = \sup_{x \neq 0} \left(\frac{\|T^K x\|}{\|x\|} \right)^{\frac{1}{K}} = \sup_{x: \|x\|=1} (\|T^K x\|)^{\frac{1}{K}} \quad (5)$$

for some finite $K \in \mathbb{N}$. This results in the optimization problem

$$\min_{\substack{L_i, i=1,2,\dots,S \\ \text{sparsity of } L_i}} \sup_{x: \|x\|=1} \|T^K x\|. \quad (6)$$

3.2 Numerical evaluation of the loss function

We denote the action of evaluating the GNN by $f^{(\theta)}$ (where θ represents the network parameters), and consider a discretized problem with DoF set D , of size n . The set D can be decomposed into subdomains either by using fixed geometric choices of the subdomain (e.g., for finite-difference

discretizations), using the METIS graph partitioner Karypis and Kumar [1998], or a k -means-based clustering algorithm (best known as Lloyd’s algorithm which has $O(n)$ time complexity) Bell [2008], Lloyd [1982]. For unstructured problems, we use a k -means-based algorithm, decomposing D to subdomains D_i for $i = 1, 2, \dots, S$, with overlap δ ; see Supplementary Materials for details. The GNN then takes D and its decomposition as inputs, as well as sparsity constraints on the matrices L_i for $i = 1, 2, \dots, S$, and outputs values for these matrices:

$$L_1^{(\theta)}, L_2^{(\theta)}, \dots, L_S^{(\theta)} \leftarrow f^{(\theta)}(D). \quad (7)$$

Using the learned subdomain interface matrices, we then obtain the modified MLORAS (Machine Learning Optimized Restricted Additive Schwarz) operator, $M_{\text{ORAS}}^{(\theta)}$, simply using $\tilde{A}_i^\delta = A_i + L_i^{(\theta)}$ in (4). We denote the associated error propagation operator by $T^{(\theta)} = I - M_{\text{ORAS}}^{(\theta)}A$.

While Gelfand’s formula and the associated upper bound in (5) are valid in any norm, it is natural to consider them with respect to the ℓ^2 norm in this setting. However, this raises the same issue as encountered in Luz et al. [2020], that it generally requires an eigendecomposition to compute the norm. To avoid this, we use a stochastic sampling of $\|(T^{(\theta)})^K\|$, generated by the sample set $X \in \mathbb{R}^{n \times m}$ for some $m \in \mathbb{N}$, given as

$$X = [x_1, x_2, \dots, x_m], \forall_j x_j \sim \mathbb{R}^n \text{ uniformly}, \|x_j\| = 1. \quad (8)$$

Here, we randomly select m points uniformly on a unit sphere in \mathbb{R}^n , which can be done using the method in Box [1958]. We then define

$$Y^{(\theta)} = \left\{ \left\| (T^{(\theta)})^K x_1 \right\|, \left\| (T^{(\theta)})^K x_2 \right\|, \dots, \left\| (T^{(\theta)})^K x_m \right\| \right\}, \quad (9)$$

taking each column of X as the initial guess to the solution of the homogeneous problem $Ax = 0$ and taking K steps of the stationary algorithm to generate $(T^{(\theta)})^K x_j$. Since we normalize each column of X to have $\|x_j\| = 1$, the value of $\|(T^{(\theta)})^K x_j\|$ serves as a lower bound for $\|(T^{(\theta)})^K\|$. Thus, taking the maximum of the values in Y provides a practical loss function that we use below, defining

$$\mathcal{L}^{(\theta)} = \max(Y^{(\theta)}). \quad (10)$$

We note similarities between this loss function and that used in Katrutsa et al. [2020], but that we are able to use the maximum of $Y^{(\theta)}$ (giving a better approximation to the norm) in our context instead of averaging.

Ultimately, the cost of our algorithm depends strongly on the chosen values of m and K . For sufficiently large values of m , we now show that the maximum value in $Y^{(\theta)}$ is an arbitrarily good approximation to $\|(T^{(\theta)})^K\|^{\frac{1}{K}}$ (in the statistical sense).

Theorem 1. *For any nonzero matrix T , $\epsilon > 0$, and $\delta < 1$, there exist $M, K \in \mathbb{N}$ such that for any $m > M$, if one chooses m points, x_j , uniformly at random from $\{x \in \mathbb{R}^n, \|x\| = 1\}$, then $Y = \{\|T^K x_1\|, \|T^K x_2\|, \dots, \|T^K x_m\|\}$ satisfies*

$$P\left(\left|\rho(T) - \max(Y)^{\frac{1}{K}}\right| < \epsilon\right) > 1 - \delta. \quad (11)$$

Proof. According to Gelfand’s theorem, there exists $L \in \mathbb{N}$ such that $\forall \ell > L$, $\left|\rho(T) - \sup_{x: \|x\|=1} \|T^\ell x\|^{\frac{1}{\ell}}\right| < \frac{\epsilon}{2}$. Take any $K \geq L$ and let $\tilde{\epsilon} = \frac{\epsilon}{2\|T^K\|^{\frac{1}{K}}}$. Since \mathbb{R}^n is finite-dimensional, there exists an $x^* \in \mathbb{R}^n$, $\|x^*\| = 1$ such that $\sup_{x: \|x\|=1} \|T^K x\| = \|T^K x^*\|$. Denote the volume of the surface of the n -dimensional sphere of unit radius around the origin in \mathbb{R}^n by C_{tot} , and the volume of the region on this sphere within radius $\tilde{\epsilon}^K$ of x^* by $C_{\tilde{\epsilon}, K}$.

Given $\delta < 1$, let $M \in \mathbb{N}$ satisfy $M \geq \frac{\log(\delta)}{\log\left(1 - \frac{C_{\tilde{\epsilon}, K}}{C_{\text{tot}}}\right)}$. Then,

$$P\left(\|x^* - x_i\| > \tilde{\epsilon}^K \text{ for all } i\right) < \left(1 - \frac{C_{\tilde{\epsilon}, K}}{C_{\text{tot}}}\right)^M \leq \delta. \quad (12)$$

Thus, with probability of at least $1 - \delta$, we expect at least one point from a selection of $m > M$ points uniformly distributed on the sphere of radius unit radius to be in $C_{\tilde{\epsilon}, K}$. Let that point be x_r , giving

$$\|T^K x^*\|^{\frac{1}{K}} - \|T^K x_r\|^{\frac{1}{K}} \leq (\|T^K x^*\| - \|T^K x_r\|)^{\frac{1}{K}} \quad (13)$$

$$\leq (\|T^K(x^* - x_r)\|)^{\frac{1}{K}} \quad (14)$$

$$\leq \|T^K\|^{\frac{1}{K}} \|x^* - x_r\|^{\frac{1}{K}} \leq \|T^K\|^{\frac{1}{K}} \tilde{\epsilon} = \frac{\epsilon}{2} \quad (15)$$

using Lemma 3 (see Supplementary Materials) and the reverse triangle inequality. Finally, by the triangle inequality, with probability of at least $1 - \delta$, we have:

$$\left| \rho(T) - \max(Y)^{\frac{1}{K}} \right| \leq \left| \rho(T) - \sup_{x: \|x\|=1} \|T^K x\|^{\frac{1}{K}} \right| + \left| \sup_{x: \|x\|=1} \|T^K x\|^{\frac{1}{K}} - \max(Y)^{\frac{1}{K}} \right| \leq \epsilon. \quad (16)$$

□

Remark. According to Loukas [2019], since the optimal interface values are Turing-computable, if the depth of the GNN is at least the diameter of the graph, and a TAGConv layer followed by a feature encoder is Turing-complete, the optimal interface values can be learned. In our setting, for a problem on a structured grid of size $N \times N$ with two identical rectangular subdomains, this implies that the GNN will be able to learn the optimal interface values given, if and only the GNN has depth at least $2N$, has deep enough feature encoders, and the width of the layers is unbounded.

Remark. Theorem 1 guarantees convergence of the loss function to the spectral radius, in the limits of many samples and many stationary iterations. To the best of our knowledge, such a guarantee is not known for the previous loss functions used in the area Luz et al. [2020], Greenfeld et al. [2019]. Moreover, there are substantial improvements in the numerical results using the new loss function in comparison to that of Luz et al. [2020], as shown in Figure 6.

Theorem 2. Assuming bounded subdomain size, the time complexity to evaluate the optimal Schwarz parameters using our method is $O(n)$, where n is the number of nodes in the grid.

Proof. Given bounded Lloyd subdomain size and fixed number of Lloyd aggregation cycles, subdomain generation has $O(n)$ time complexity Bell [2008] (see the Supplementary Material). To evaluate each TAGConv layer, one computes $y = \sum_{\ell=1}^L G_{\ell} x_{\ell} + b \mathbf{1}_n$, where L is the number of node features, $G_{\ell} \in \mathbb{R}^{n \times n}$ is the graph filter, b is a learnable bias, and $x_{\ell} \in \mathbb{R}^n$ are the node features. Moreover, the graph filter is a polynomial in the adjacency matrix M of the graph: $G_{\ell} = \sum_{j=0}^J g_{\ell,j} M^j$ where J is a constant and $g_{\ell,j}$ are the coefficients of filter polynomial. Since the graph has bounded node degrees, it implies that M is sparse and the action of M^j has $O(n)$ cost, and therefore, the full TAGConv evaluation also has $O(n)$ cost. Moreover, the cost of edge feature and the feature networks are $O(n)$, resulting in overall $O(n)$ cost. □

3.3 Training Details

We use a graph neural network based on four TAGConv layers and ResNet node feature encoders consisting of eight blocks after each TAGConv layer; see Supplementary Materials for more details on the structure of the GNN, and Section 4.3 for an ablation study. The training set in our study consists of 1000 unstructured grids with piecewise linear finite elements and with grids ranging from 90–850 nodes (and an average of 310 nodes). The grids are generated by choosing either a regular grid (randomly selected 60% of the time) or a randomly generated convex polygon; pygmsh Schlömer [2021] is used to generate the mesh on the polygon interior. A sample of the training grids is shown in Figure 2. We train the GNN for four epochs with a mini batch size of 25 using the ADAM optimizer Kingma and Ba [2014] with a fixed learning rate of 10^{-4} . For the numerical evaluation of the loss function (10) we use $K = 4$ iterations and $m = 500$ samples. The code¹ was implemented using PyTorch Geometric Fey and Lenssen [2019], PyAMG Bell et al. [2022], and NetworkX Hagberg et al. [2008]. All training was performed on an 8-core i9 Macbook Pro using CPU only.

¹All code and data for this paper is at <https://github.com/compdyn/learning-oras> (MIT licensed).

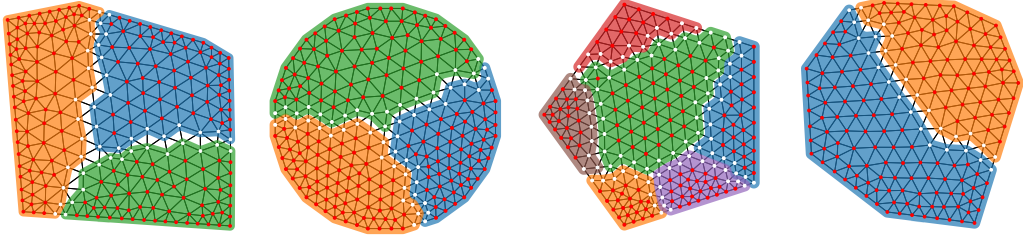


Figure 2: Example grids from the training set.

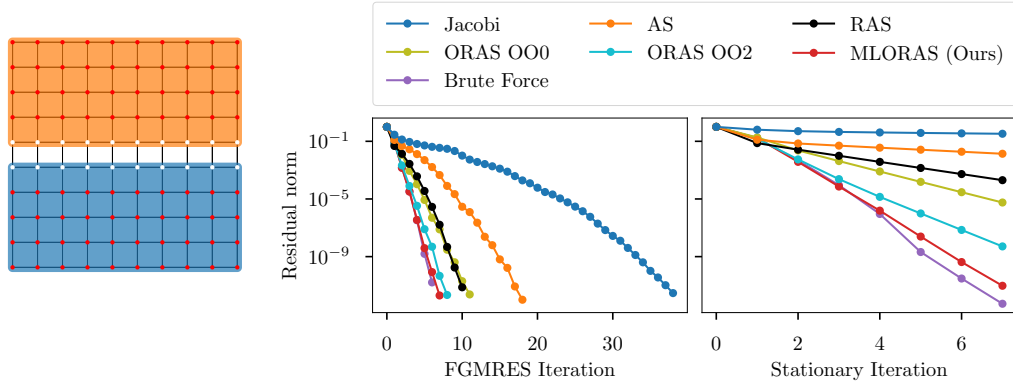


Figure 3: Results for the Helmholtz problem on a 10×10 structured grid (left) with two identical subdomains, with convergence plots for the methods used as preconditioners for FGMRES (center) and as stationary algorithms (right).

Moreover, we train two special networks for use in Section 4.1. The first is a “Brute Force” network, which is a single-layer neural network without an activation function, trained only on a structured 10×10 grid with two identical subdomains using the ADAM optimizer. The purpose of training this is to obtain the optimal interface values as a benchmark for comparison, including against our method. The second is the same network used for our method, MLORAS, but overtrained on only the problem in Section 4.1, to understand the learning capabilities of the method and choice of GNN architecture.

4 Results

4.1 Two-subdomain structured grids

We first consider rectangular structured grids with two subdomains. Although restrictive, these problems allow us to directly compare to existing OSM parameters, which are only available for structured grids and exactly two subdomains. We follow St-Cyr et al. [2007] and consider the Helmholtz problem (1) on the unit square with $\eta = 1$ and homogeneous Dirichlet boundary conditions. We discretize the problem on an $N \times N$ rectangular grid with $h = 1/(N + 1)$ grid spacing, using the standard five-point finite difference stencil.

Figure 3 shows the results of different methods on a 10×10 structured grid with two identical subdomains. We see that the overtrained MLORAS network learns interface parameters that outperform the Restrictive Additive Schwarz (RAS) Cai and Sarkis [1999] method; more significantly, MLORAS also outperforms the existing Optimized-RAS (ORAS) methods that were analytically derived for this specific problem (zeroth-order OO0 and second-order OO2 from St-Cyr et al. [2007]). Moreover, in these results, the MLORAS network almost reaches the performance of the “Brute Force” network (obtained by directly optimizing all interface values for this single structured grid), indicating that using a GNN to encode the optimal interface values does not significantly restrict the search space.

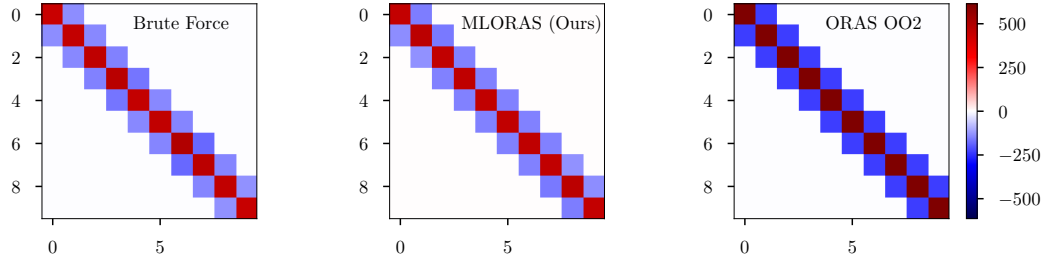


Figure 4: Interface values for the 10×10 structured grid with two identical subdomains. From left to right: brute force optimization of the interface values, MLORAS, and second-order ORAS (OO2) St-Cyr et al. [2007].

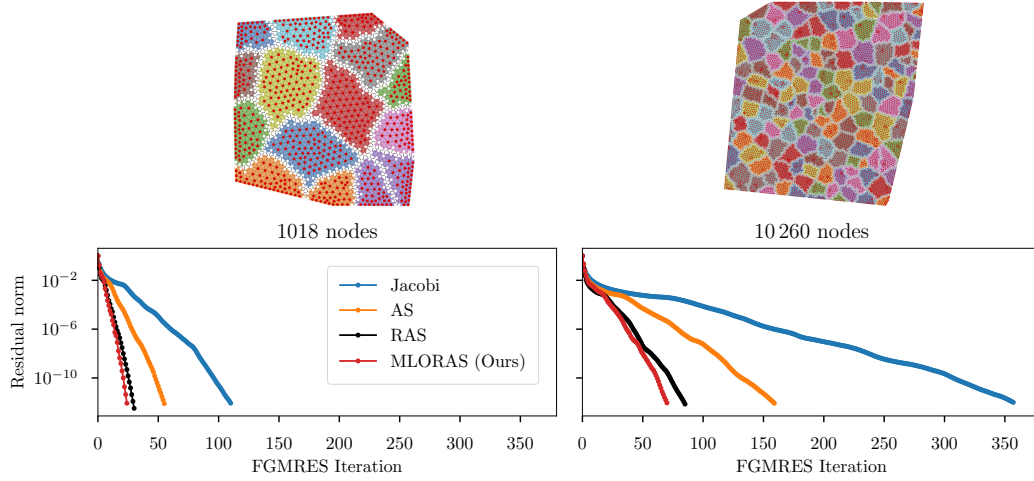


Figure 5: Example convergence on smaller (left) and larger (right) unstructured grids.

To understand the performance of the methods in more detail, Figure 4 plots the interface values output by the brute force optimization, the MLORAS network, and the OO2 ORAS algorithm. This shows that the MLORAS network is choosing interface values very close to those directly optimized by the brute force method, unlike those selected by the OO2 method.

4.2 Unstructured grids

To evaluate the performance of the MLORAS network on unstructured grids, we consider 16 unstructured triangular grids in 2D with sizes ranging from about 90 to 40 000 nodes. These grids are defined on convex subsets of $(0, 1) \times (0, 1)$; we solve the Helmholtz problem (1) on these domains with $\eta = 1$ and homogeneous Dirichlet boundary conditions, discretized with piecewise-linear finite elements.

Example convergence plots are shown in Figure 5, where our method (MLORAS) is compared to RAS (Restricted Additive Schwarz Cai and Sarkis [1999]), AS (Additive Schwarz), and Jacobi methods as a preconditioner for FGMRES. Here we see that the MLORAS network is able to learn optimized interface parameters for unstructured grids that outperform RAS, and that MLORAS can scale to problems that are much larger than those in the training set, which are all below $n = 1000$ nodes. Importantly, MLORAS retains an advantage over RAS even as the grid size increases.

Figure 6 shows the performance of three different methods across all unstructured test grids. The three methods are: (1) “F-norm optimized”: the same network as MLORAS, but trained to directly optimize the Frobenius norm of the error propagation matrix, $\|A\|_F$, (2) the RAS Cai and Sarkis [1999] method, and (3) the MLORAS method. We do not show ORAS results here, as it cannot be applied to unstructured grids. Figure 6 reveals two important facts. First, MLORAS consistently

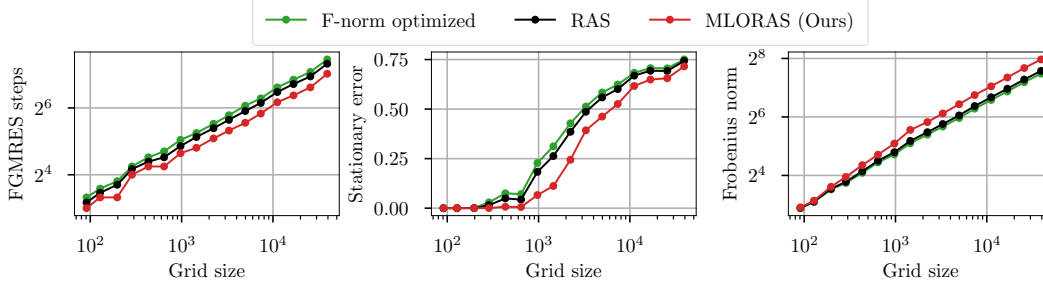


Figure 6: Convergence on all unstructured grids in the testing set. Left: the number of preconditioned FGMRES steps required to solve the problem to within a relative error of 10^{-12} . Center: error reduction by the stationary iteration after 10 iterations. Right: Frobenius norm for each method on each test problem.

outperforms RAS over the entire testing set, both as an FGMRES preconditioner and as a stationary algorithm, and this advantage is maintained even for large grids. Second, we see that the Frobenius norm is indeed a worse choice for the loss function than our new loss in (6). We see this from the fact that MLORAS has a worse Frobenius norm than either of the other two methods, but it has the best convergence rate. In addition, when we explicitly optimize the Frobenius norm (the “F-norm optimized” method), we see that we do obtain the lowest Frobenius norm, but this translates to the worst convergence rate.

4.3 Ablation study

To understand the impact of the network structure on performance, we conduct an ablation study by varying the ResNet block length and the number of TAGConv layers. In each case, we train a network on five different training sets, each consisting of 1000 grids generated as described in Section 3.3. The trained networks are tested on 50 unstructured grids, each with 2400 to 2600 nodes. For each architecture, the mean performance is computed, together with error bars from the fivefold repetition, with results shown in Figure 7. We see that a higher residual block length is always better, but that the optimal number of TAGConv layers is 4, and using more layers actually decreases performance. This phenomenon has been observed in other contexts (e.g., Zhao and Akoglu [2019] and Chen et al. [2020]) and can be attributed to over-smoothing in GNNs. The use of residual blocks in our architecture is, thus, important to allow us to increase network depth without needing to increase the number of GNN layers.

5 Conclusion

We propose an unsupervised learning method based on Graph Convolutional Neural Networks (GCNNs) for extending optimized restricted additive Schwarz (ORAS) methods to multiple subdomains and unstructured grid cases. Our method is trained with a novel loss function, stochastically minimizing the spectral radius of the error propagation operator obtained using the learned interface values. The time complexity of evaluating the loss function, as well as obtaining the interface values using our neural network are all linear in problem size. Moreover, the proposed method is able to outperform ORAS, both as a stationary algorithm and preconditioner for FGMRES on structured grids with two subdomains, as considered in the conventional ORAS literature. On more general cases, such as unstructured grids with arbitrary subdomains of bounded size, our method outperforms RAS consistently, both as a stationary algorithm and preconditioner for FGMRES. The main limitations of the current work are that the method was studied for two PDE cases, namely the Helmholtz problem in the main paper and the non-uniform Poisson problem in Appendix D. We also defer the study of nonlinear or time-dependent PDEs to future work.

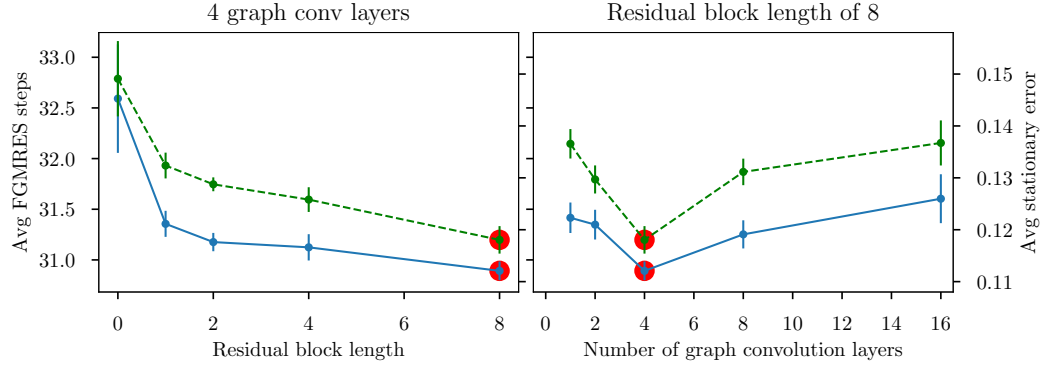


Figure 7: Ablation study results. The left panel varies the residual block length while keeping the number of TAGConv layers fixed at 4. The right panel varies the number of TAGConv layers while keeping the residual block length fixed at 8. The solid blue lines (left axis) show the average number of FGMRES steps needed to reduce the relative error below 10^{-12} , while the dashed green lines (right axis) show the average stationary algorithm error reduction after 10 iterations. The red circles mark the results for the network with the best performance (residual block length of 8 and 4 TAGConv layers), which was used for all other studies in this paper. Error bars show one standard error of the mean.

Acknowledgement

The work of S.P.M. was partially supported by an NSERC Discovery Grant. The authors thank the referees for their insightful comments. The authors have no competing interests to declare.

References

- Andrea Toselli and Olof Widlund. *Domain decomposition methods—algorithms and theory*, volume 34 of *Springer Series in Computational Mathematics*. Springer-Verlag, Berlin, 2005. ISBN 3-540-20696-5. doi: 10.1007/b137868.
- Alfio Quarteroni and Alberto Valli. *Domain decomposition methods for partial differential equations*. Numerical Mathematics and Scientific Computation. The Clarendon Press, Oxford University Press, New York, 1999. ISBN 0-19-850178-1. Oxford Science Publications.
- Victorita Dolean, Pierre Jolivet, and Frédéric Nataf. *An introduction to domain decomposition methods*. Society for Industrial and Applied Mathematics (SIAM), Philadelphia, PA, 2015. ISBN 978-1-611974-05-8. doi: 10.1137/1.9781611974065.ch1.
- M.J. Gander, L. Halpern, and F. Nataf. Optimized Schwarz methods. In *Proceedings of the 12th International Conference on Domain Decomposition*, pages 15–27. ddm.org, 2000.
- Martin J. Gander and Felix Kwok. Optimal interface conditions for an arbitrary decomposition into subdomains. In *Domain decomposition methods in science and engineering XIX*, volume 78 of *Lect. Notes Comput. Sci. Eng.*, pages 101–108. Springer, Heidelberg, 2011. doi: 10.1007/978-3-642-11304-8_9.
- Xiao-Chuan Cai and Marcus Sarkis. A restricted additive Schwarz preconditioner for general sparse linear systems. *Siam Journal on Scientific Computing*, 21(2):792–797, 1999.
- Amik St-Cyr, Martin J Gander, and Stephen J Thomas. Optimized multiplicative, additive, and restricted additive Schwarz preconditioning. *SIAM Journal on Scientific Computing*, 29(6):2402–2425, 2007.
- Frédéric Magoulès, Daniel B. Szyld, and Cédric Venet. Asynchronous optimized Schwarz methods with and without overlap. *Numer. Math.*, 137(1):199–227, 2017. ISSN 0029-599X. doi: 10.1007/s00211-017-0872-z.
- Maziar Raissi, Paris Perdikaris, and George E Karniadakis. Physics-informed neural networks: A deep learning framework for solving forward and inverse problems involving nonlinear partial differential equations. *Journal of Computational Physics*, 378:686–707, 2019.
- Zongyi Li, Nikola Kovachki, Kamyar Azizzadenesheli, Burigede Liu, Kaushik Bhattacharya, Andrew Stuart, and Anima Anandkumar. Fourier neural operator for parametric partial differential equations. *arXiv preprint arXiv:2010.08895*, 2020a.
- Daniel Greenfeld, Meirav Galun, Ronen Basri, Irad Yavneh, and Ron Kimmel. Learning to optimize multigrid PDE solvers. In *International Conference on Machine Learning*, pages 2415–2423. PMLR, 2019.
- Ilay Luz, Meirav Galun, Haggai Maron, Ronen Basri, and Irad Yavneh. Learning algebraic multigrid using graph neural networks. In *International Conference on Machine Learning*, pages 6489–6499. PMLR, 2020.
- Ali Taghibakhshi, Scott MacLachlan, Luke Olson, and Matthew West. Optimization-based algebraic multigrid coarsening using reinforcement learning. *Advances in Neural Information Processing Systems*, 34, 2021.
- Alexander Heinlein, Axel Klawonn, Martin Lanser, and Janine Weber. Combining machine learning and domain decomposition methods for the solution of partial differential equations—a review. *GAMM-Mitteilungen*, 44(1):e202100001, 2021.
- Alexander Heinlein, Axel Klawonn, Martin Lanser, and Janine Weber. Machine learning in adaptive domain decomposition methods—predicting the geometric location of constraints. *SIAM Journal on Scientific Computing*, 41(6):A3887–A3912, 2019.
- Ke Li, Kejun Tang, Tianfan Wu, and Qifeng Liao. D3M: A deep domain decomposition method for partial differential equations. *IEEE Access*, 8:5283–5294, 2019.

- Wuyang Li, Xueshuang Xiang, and Yingxiang Xu. Deep domain decomposition method: Elliptic problems. In *Mathematical and Scientific Machine Learning*, pages 269–286. PMLR, 2020b.
- Valentin Mercier, Serge Gratton, and Pierre Boudier. A coarse space acceleration of deep-DDM. *arXiv preprint arXiv:2112.03732*, 2021.
- Zonghan Wu, Shirui Pan, Fengwen Chen, Guodong Long, Chengqi Zhang, and S Yu Philip. A comprehensive survey on graph neural networks. *IEEE Transactions on Neural Networks and Learning Systems*, 2020.
- Joan Bruna, Wojciech Zaremba, Arthur Szlam, and Yann LeCun. Spectral networks and locally connected networks on graphs. *arXiv preprint arXiv:1312.6203*, 2013.
- Michaël Defferrard, Xavier Bresson, and Pierre Vandergheynst. Convolutional neural networks on graphs with fast localized spectral filtering. *arXiv preprint arXiv:1606.09375*, 2016.
- Thomas N Kipf and Max Welling. Semi-supervised classification with graph convolutional networks. *arXiv preprint arXiv:1609.02907*, 2016.
- Justin Gilmer, Samuel S Schoenholz, Patrick F Riley, Oriol Vinyals, and George E Dahl. Neural message passing for quantum chemistry. In *International Conference on Machine Learning*, pages 1263–1272. PMLR, 2017.
- Peter W Battaglia, Jessica B Hamrick, Victor Bapst, Alvaro Sanchez-Gonzalez, Vinicius Zambaldi, Mateusz Malinowski, Andrea Tacchetti, David Raposo, Adam Santoro, Ryan Faulkner, et al. Relational inductive biases, deep learning, and graph networks. *arXiv preprint arXiv:1806.01261*, 2018.
- Jian Du, Shanghang Zhang, Guanhang Wu, José MF Moura, and Soumya Kar. Topology adaptive graph convolutional networks. *arXiv preprint arXiv:1710.10370*, 2017.
- Wei Wang, Zheng Dang, Yinlin Hu, Pascal Fua, and Mathieu Salzmann. Backpropagation-friendly eigendecomposition. *Advances in Neural Information Processing Systems*, 32, 2019.
- George Karypis and Vipin Kumar. A fast and high quality multilevel scheme for partitioning irregular graphs. *SIAM Journal on scientific Computing*, 20(1):359–392, 1998.
- William N Bell. *Algebraic multigrid for discrete differential forms*. PhD thesis, University of Illinois at Urbana-Champaign, 2008.
- Stuart Lloyd. Least squares quantization in PCM. *IEEE Transactions on Information Theory*, 28(2): 129–137, 1982.
- George EP Box. A note on the generation of random normal deviates. *Ann. Math. Statist.*, 29: 610–611, 1958.
- Alexandr Katrutsa, Talgat Daulbaev, and Ivan Oseledets. Black-box learning of multigrid parameters. *Journal of Computational and Applied Mathematics*, 368:112524, 2020. ISSN 0377-0427. doi: <https://doi.org/10.1016/j.cam.2019.112524>.
- Andreas Loukas. What graph neural networks cannot learn: depth vs width. *arXiv preprint arXiv:1907.03199*, 2019.
- Nico Schlömer. pygmsh: A Python frontend for Gmsh, 2021. URL <https://github.com/nschloe/pygmsh>. (GPL-3.0 License).
- Diederik P Kingma and Jimmy Ba. Adam: A method for stochastic optimization. *arXiv preprint arXiv:1412.6980*, 2014.
- Matthias Fey and Jan E. Lenssen. Fast graph representation learning with PyTorch Geometric. In *ICLR Workshop on Representation Learning on Graphs and Manifolds*, 2019. (code is MIT licensed).

- Nathan Bell, Luke N. Olson, and Jacob Schroder. PyAMG: Algebraic multigrid solvers in python. *Journal of Open Source Software*, 7(72):4142, 2022. doi: 10.21105/joss.04142. URL <https://doi.org/10.21105/joss.04142>. (code is MIT licensed).
- Aric Hagberg, Pieter Swart, and Daniel S Chult. Exploring network structure, dynamics, and function using networkx. Technical report, Los Alamos National Lab.(LANL), Los Alamos, NM (United States), 2008. (code is BSD licensed).
- Lingxiao Zhao and Leman Akoglu. Pairnorm: Tackling oversmoothing in GNNs. *arXiv preprint arXiv:1909.12223*, 2019.
- Deli Chen, Yankai Lin, Wei Li, Peng Li, Jie Zhou, and Xu Sun. Measuring and relieving the oversmoothing problem for graph neural networks from the topological view. In *Proceedings of the AAAI Conference on Artificial Intelligence*, volume 34, pages 3438–3445, 2020.
- Thomas H Cormen, Charles E Leiserson, Ronald L Rivest, and Clifford Stein. *Introduction to algorithms (Second edition)*. MIT Press, 2001.

Appendix A Useful lemma

This lemma is useful in the proof of Theorem 1. While its proof is quite simple, we are not aware of the result in the literature, and include it here for completeness.

Lemma 3. For $x, y \in \mathbb{R}$, with $0 \leq y \leq x$ and any $K \in \mathbb{N}$, $x^{\frac{1}{K}} - y^{\frac{1}{K}} \leq (x - y)^{\frac{1}{K}}$

Proof. Since $y \leq x$, the binomial theorem gives that

$$x \leq (x - y) + y + \sum_{i=1}^{K-1} \binom{K}{i} y^{\frac{i}{K}} (x - y)^{\frac{K-i}{K}} = (y^{\frac{1}{K}} + (x - y)^{\frac{1}{K}})^K. \quad (17)$$

Taking the K^{th} root of both sides and rearranging gives the stated result. \square

Appendix B Solution plots

We have compared the solution plot of our method with RAS for the Holmholtz problem. We consider a 100×100 structured grid on the $(0, 1) \times (0, 1)$ domain, and consider the following true solution for the problem: $u^* = \sin(8\pi x) + \sin(8\pi y)$. We then start with an initial random guess with L_2 norm of 1. We apply 10 iterations of RAS and MLORAS (ours) as stationary algorithm and obtain solution for each method. Moreover, we run 10 iterations of FGMRES with MLORAS and RAS preconditioners on the initial guess and obtain predictions for both methods. The results are shown in Figure 8 for MLORAS and Figure 9 for RAS.

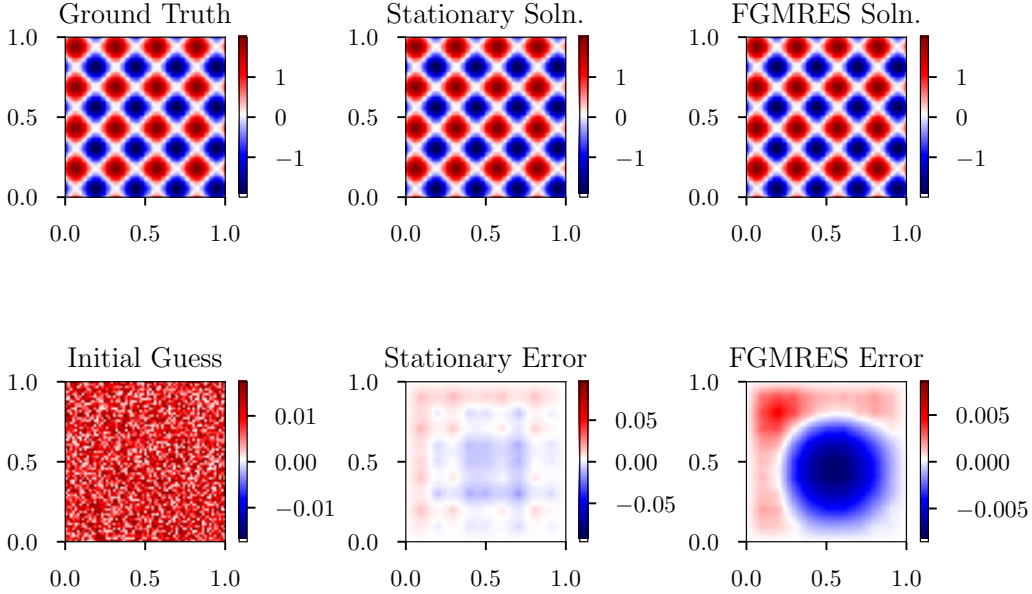


Figure 8: MLORAS (ours) solution plots. Top left: ground truth, top middle: MLORAS stationary solution after 10 iterations, top right: FGMRES solution with MLORAS preconditioner after 10 steps, bottom left: initial guess, bottom middle: error of MLORAS stationary solution (L_2 norm of error = 0.231), bottom right: error of FGMRES with MLORAS preconditioner solution (L_2 norm of error = 0.084).

Appendix C Neural network

C.1 Inputs and Output

Inputs: The GNN takes the grid G as its input which has three main components, namely D_{node} (node feature matrix), D_{edge} (edge feature matrix), and A (the graph adjacency matrix). Every node

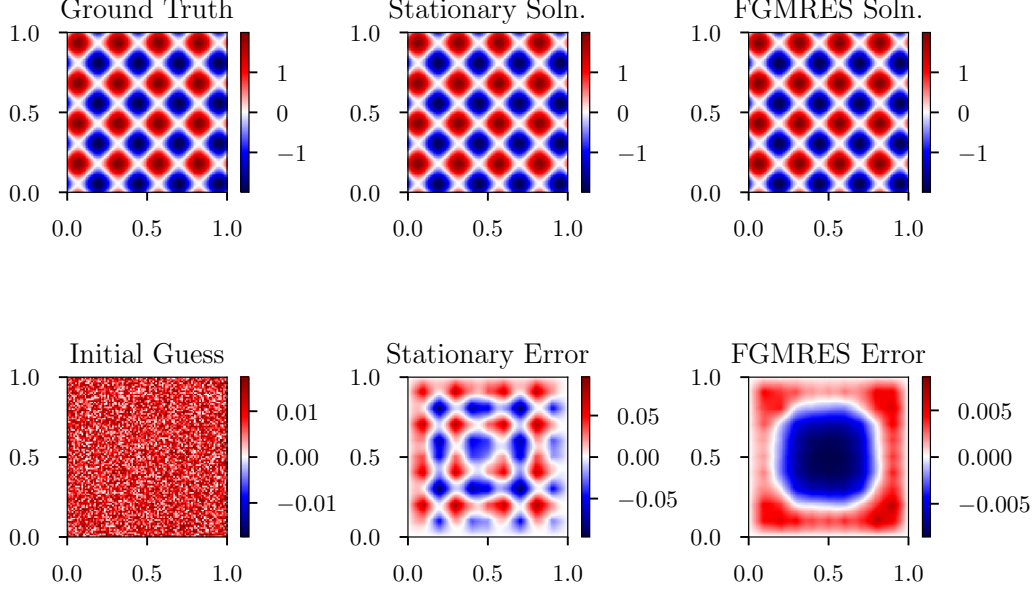


Figure 9: RAS solution plots. Top left: ground truth, top middle: RAS stationary solution after 10 iterations, top right: FGMRES solution with RAS preconditioner after 10 steps, bottom left: initial guess, bottom middle: error of RAS stationary solution (L_2 norm of error = 6.526), bottom right: error of FGMRES with RAS preconditioner solution (L_2 norm of error = 0.146).

has a binary feature, and its value is one if it is on a boundary of a subdomain and zero otherwise. Therefore, for every node, the corresponding element in D_{node} indicates whether that point is on a boundary or not. In other words, the binary node feature determines the grid decomposition. D_{edge} consists of the edge values obtained from discretization of the underlying PDE.

Outputs: After passing the input to the GNN architecture which consists of node and edge convolution blocks and is fully described in the following subsection, the learned edge weights are obtained for every edge in the grid. However, only the edges between the nodes on the subdomain boundaries (considering self-loops) are of our interest so we mask the rest of the edges. Therefore, the output of the GNN is the learned values for edges connecting nodes on the boundary of a subdomain which are referred to as interface values in the paper. For the i -th subdomain, the interface value matrix is referred to as L_i^θ , where θ represents the GNN learnable parameters (see Equation 7). Figure 3 shows an example of the sparsity pattern of an L matrix for each of the identical subdomains of the 10×10 structured grid in Figure 4. Also note that the interface values are the nonzero elements of the corresponding L matrix.

C.2 Architecture

The overall architecture of the GNN is shown in Figure 10. The GNN takes a graph as its input and sends node and edge features to the node convolution and edge feature preprocessing blocks, respectively, both of which are shown in Figure 11. Each node convolution block consists of a TAGConv layer with 2-size filters and 128 hidden units, followed by a ReLU activation, an instance norm layer, and a feature network block. The feature network block, as shown in Figure 12, consists of 8 blocks with residual connections between each; furthermore, each of the blocks consists of a layer norm followed by a fully connected layer of size 128, followed by a ReLU activation, and finally another fully connected layer of size 128. The edge feature preprocessing block takes the edge features and applies fully connected layers, ReLU nonlinearities, and instance normalization, before the graph convolution pass.

After passing through all of the node convolution blocks, the edge and node features are sent to a stack block. This block simply stacks node features onto the edges adjacent to each node. For every edge,

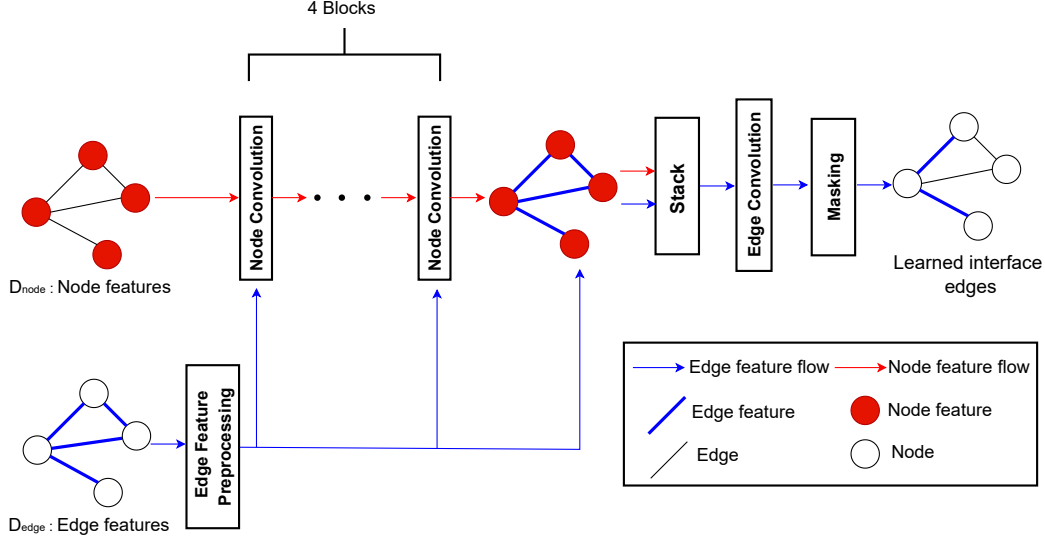


Figure 10: Overall GNN architecture.

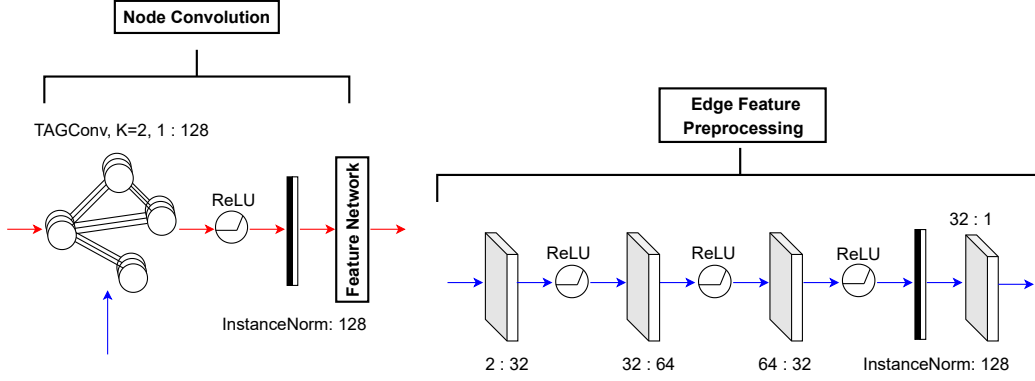


Figure 11: Left: Node convolution block. Right: Edge feature preprocessing block.

(u, v) , where u and v are the nodes on that edge, denote the node and edge features by $E_u, E_v, E_{(u,v)}$, which are the inputs to the stack block. The block then stacks these features and outputs them as the new edge features for the edge (u, v) . Following the stack layer is the edge convolution block, depicted in Figure 13, which takes the stacked edge and node features and passes them through a series of fully connected layers, ReLU activation functions, and layer norms. It is noteworthy that the size of the input to the edge convolution block is 257, since following the description of the stack block, the two node features, each of size 128, and the edge feature of size 1 are stacked together. The output from the edge convolution block is, finally, passed through a masking block that outputs the interface values. This masks the interior edge values, i.e., takes the output of the GNN (one value per each edge in the graph) and multiplies those values that are not on the boundary of a subdomain by zero, to restrict the output from the GNN to the desired edges in the graph.

Appendix D Poisson problem with discontinuous diffusion coefficient

We also consider the 2D Poisson problem with discontinuous diffusion coefficient which is formulated as follows:

$$-\nabla \cdot \kappa(x, y) \nabla u = f \quad \text{in } \Omega, \quad \kappa(x, y) = \begin{cases} 1000 & 0 < x < 0.5 \\ 1 & 0.5 \leq x < 1. \end{cases} \quad (18)$$

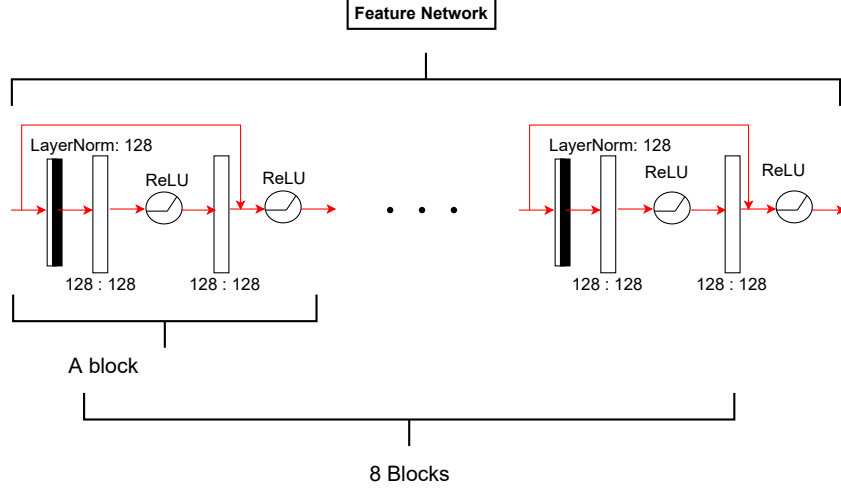


Figure 12: Feature network blocks.

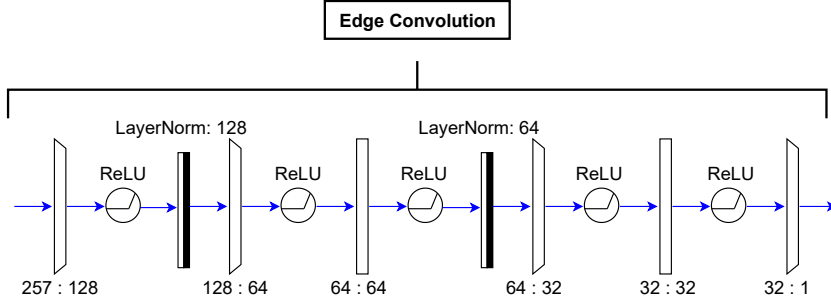


Figure 13: Edge convolution block.

where Ω is, as before, defined as a convex subset of $(0, 1) \times (0, 1)$ and $\kappa(x, y)$ is the discontinuous diffusion coefficient. For this problem, we consider nine domains with unstructured triangular grids, with sizes ranging from about 100 to over 30k nodes. The subdomains are generated using Lloyd aggregation (fully explained in Appendix E), with a fixed ratio of 0.015. We note that the subdomains are not constrained in any way, and a single subdomain may contain parts of the domain with different diffusion coefficients. The results of our method compared with RAS baseline for both the stationary algorithm and the FGMRES preconditioner are shown in Figure 14, and show little qualitative difference with the earlier results for Helmholtz.

Appendix E Lloyd aggregation

Lloyd’s algorithm Lloyd [1982] is a standard approach for partitioning data, closely related to k -means clustering, that can be used (for example) to find close approximations to centroidal Voroni tessellations. Here, we use a modified form of Lloyd’s algorithm, known as Lloyd aggregation Bell [2008], to partition a given set of degrees of freedom, V , into the non-overlapping subdomains, V_i^0 , for $i \in \{1, 2, \dots, S\}$, needed as input to our algorithm. (Note that, here, we change notation from the paper and use V to denote the vertices in the graph associated with the matrix, rather than D to denote the index set of degrees of freedom.) Consider a 2D planar graph, G , the set of all edges E , the set of all of its nodes V , and $V_c \subseteq V$. The nodes in V_c serve as the centers of “clusters” in the graph that will define the subdomains, V_i^0 . These regions are obtained based on the closest center to each graph node, where the distance is measured by the number of edges covered in the shortest path between two nodes (denote distance in the graph between node i and j by g_{ij}). Define the centroid of a region as the farthest node from the boundary, breaking possible ties by random choice. We use a modified version of the Bellman-Ford algorithm, commonly used for obtaining the nearest center

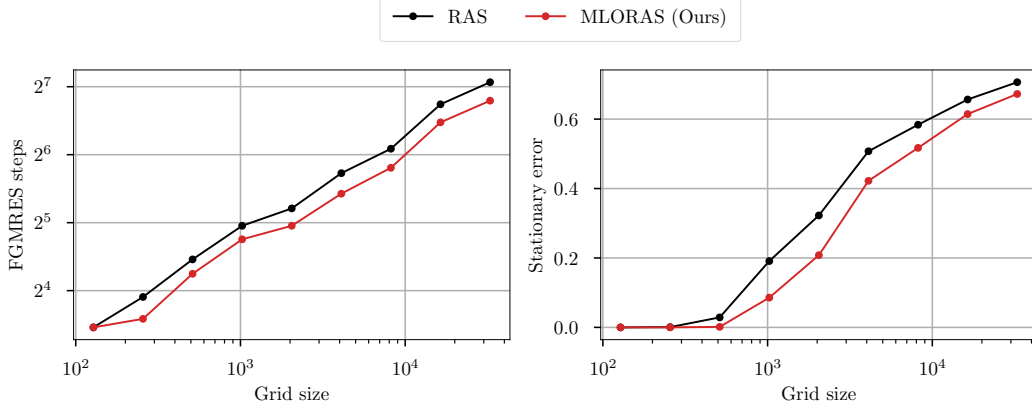


Figure 14: Discontinuous diffusion coefficient for Poisson problem on various size grids. Left: the number of preconditioned FGMRES steps required to solve the problem to within a relative error of 10^{-12} . Right: error reduction by the stationary iteration after 10 iteration.

to every node in V and its associated distance Cormen et al. [2001]. Let \vec{n} be a list of graph nodes whose i -th element is the nearest center to the i -th node of the graph, and let g_j be the graph distance from node j to n_j ; then, the modified Bellman-Ford algorithm is shown in Algorithm 1.

Algorithm 1 Modified Bellman-Ford

```

1: Input  $E$ : The set all edges,  $V$ : The set of all nodes,  $V_c$ : The set of initial center nodes.
2:  $g_i = \infty \ \forall_{i \in \{1, 2, \dots, |V|\}}$ 
3:  $n_i = -1 \ \forall_{i \in \{1, 2, \dots, |V|\}}$ 
4: for  $c \in V_c$  do
5:    $g_c \leftarrow 0$ 
6:    $n_c \leftarrow c$ 
7: end for
8: while True do
9:   Finished  $\leftarrow$  True
10:  for  $(i, j) \in E$  do
11:    if  $g_i + g_{ij} < g_j$  then
12:       $g_j \leftarrow g_i + g_{ij}$ 
13:       $n_j \leftarrow n_i$ 
14:    end if
15:  end for
16:  if Finished then
17:    return  $\vec{g}, \vec{n}$ 
18:  end if
19: end while

```

While this is an iterative computation, it has finite termination when the values in \vec{g} and \vec{n} stop changing. After running this modified Bellman-Ford algorithm, Lloyd's algorithm modifies the clusters by selecting the centroid of every subdomain as its new center, then iterates, using the modified Bellman-Ford algorithm to calculate new distances and nearest centers. Given updated center positions, it forms the new subdomains. The full Lloyd algorithm is shown in Algorithm 2, where we define the set of border nodes, B , as the set of all nodes that are connected by an edge to a node that has a different nearest center node. The key point here is that we use Modified Bellman-Ford to assign closest centers, then compute the set of border nodes, then find the new centers as those that are further from the border set within each of the original subdomains (using graph distances from B , but original center assignment in \vec{n}).

Algorithm 2 Lloyd Aggregation

```
1: Input  $K$ : Number of iterations,  $E$ : The set of all edges,  $V$ : The set of all nodes,  $V_c$ : The set of  
   initial center nodes.  
2: for  $i = 1, 2, 3, \dots, K$  do  
3:    $\vec{g}, \vec{n} \leftarrow \text{Modified Bellman-Ford}(E, V, V_c)$   
4:    $B \leftarrow \emptyset$   
5:   for  $(i, j) \in E$  do  
6:     if  $n_i \neq n_j$  then  
7:        $B \leftarrow B \cup \{i, j\}$   
8:     end if  
9:   end for  
10:   $\vec{g}, \vec{x} \leftarrow \text{Modified Bellman-Ford}(E, V, B)$   
11:   $V_c \leftarrow \{i \in V : g_i > g_j \ \forall n_i = n_j\}$   
12: end for  
13: return  $\vec{n}$ 
```

Time Complexity: Assuming each node's initial distance to a center node is bounded independently of $|V|$, and also assuming that each node's degree is bounded independently of $|V|$, Algorithm 1 runs a $|V|$ -independent number of iterations to determine one nearest center node for every point. Thus, Algorithm 1 is $O(|V|)$ in our case. This is run a $|V|$ -independent number of times in Algorithm 2, to generate the subdomains, resulting in an overall algorithmic cost of $O(|V|)$.